Check for updates

Optimal Selection of Basis Functions for Robust Tracking Control of Uncertain Linear Systems—With Application to **Three-Dimensional Printing**

Keval S. Ramani

Mem. ASME Smart and Sustainable Automation Research Lab. Department of Mechanical Engineering, University of Michigan, 2350 Hayward, Ann Arbor, MI 48109 e-mail: ksramani@umich.edu

Chinedum E. Okwudire¹

Mem. ASME Smart and Sustainable Automation Research Lab, Department of Mechanical Engineering, University of Michigan, 2350 Hayward, Ann Arbor, MI 48109 e-mail: okwudire@umich.edu

There is growing interest in the use of the filtered basis functions (FBF) approach to track linear systems, especially nonminimum phase (NMP) plants, because of its distinct advantages compared to other tracking control methods in the literature. The FBF approach expresses the control input to the plant as a linear combination of basis functions with unknown coefficients. The basis functions are forward filtered through the plant dynamics, and the coefficients are selected such that tracking error is minimized. Similar to other feedforward control methods, the tracking accuracy of the FBF approach deteriorates in the presence of uncertainties. However, unlike other methods, the FBF approach presents flexibility in terms of the choice of the basis functions, which can be used to improve its accuracy. This paper analyzes the effect of the choice of the basis functions on the tracking accuracy of FBF, in the presence of uncertainties, using the Frobenius norm of the lifted system representation (LSR) of FBF's error dynamics. Based on the analysis, a methodology for optimal selection of basis functions to maximize robustness is proposed, together with an approach to avoid large control effort when it is applied to NMP systems. The basis functions resulting from this process are called robust basis functions. Applied experimentally to a desktop three-dimensional (3D) printer with uncertain NMP dynamics, up to 48% improvement in tracking accuracy is achieved using the proposed robust basis functions compared to B-splines, while utilizing much less control effort. [DOI: 10.1115/1.4051097]

1 Introduction

Tracking control is a fundamental problem encountered in a wide range of fields such as manufacturing, robotics, automotive, and aeronautics. The objective of tracking control is to force the output trajectory of the controlled system to follow a desired trajectory as closely as possible. Tracking control could be achieved using feedforward and/or feedback controllers. This paper is written in the context of feedforward tracking control of discrete-time linear systems and is motivated by: (i) applications where feedforward is the only recourse due to lack or inadequacy of feedback sensors, for example, stepper motor driven threedimensional (3D) printers, and (ii) applications where feedforward control plays a larger role in tracking control as compared to feedback control, for example, in wafer scanning stages where 99% of the control effort required for tracking is generated by feedforward [1].

Feedforward tracking control of linear systems can be ideally achieved using perfect tracking control, i.e., pole-zero cancelation [2]. However, in practice, ideal feedforward control cannot be realized due to (i) nonminimum phase (NMP) zeros and (ii) uncertainty in the plant dynamics [3]. When applied to NMP systems, perfect tracking control results in highly oscillatory or unbounded control trajectories which are unacceptable. NMP zeros are quite prevalent in practice. For example, they occur in systems with fast sampling rates [4], as well as in systems with noncollocated placement of sensors and actuators [5]. Hence, a lot of research on feedforward tracking control of NMP systems can be found in the

Contributed by the Dynamic Systems Division of ASME for publication in the JOURNAL OF DYNAMIC SYSTEMS, MEASUREMENT, AND CONTROL. Manuscript received July 16, 2020; final manuscript received May 3, 2021; published online June 7, 2021. Assoc. Editor: Douglas Bristow.

literature (Refs. [6–8] present detailed literature reviews on the subject). Recently, the filtered basis functions (FBF) approach has been gaining attention as an effective approach for feedforward tracking control of linear NMP systems [9-13]. The FBF approach expresses the control input as a linear combination of user-defined basis functions (of which there are a wide range of choices, e.g., B-splines [9], cosine signals [14], radial basis functions [11], etc.). The basis functions are forward filtered through the plant dynamics, and the coefficients are selected, using an elegant least squares solution, such that the tracking error is minimized. The FBF approach finds its origins in iterative learning control [14] but was not applied to feedforward tracking control of NMP systems until recently [9–13]. Unlike most of the methods in the literature, the FBF approach is effective for a wide range of desired trajectories and plants including nonhyperbolic systems (systems with zeros on the unit circle in the z-plane) [10,13], square and nonsquare multi-input multi-output systems, linear time-varying (LTV) systems, linear parameter varying systems [11], etc. Also, the tracking accuracy of FBF does not change significantly with plant dynamics, as compared to other popular methods in the literature

A key challenge of feedforward controllers, including FBF, is how to improve their robustness in the presence of uncertainty in plant dynamics [3,16-21]. The tracking accuracy of feedforward methods such as FBF can be improved by complementing them with some form of feedback control, for example, real-time feedback [16,22,23], adaptive control [17], iterative learning control [24-28], etc. However, as mentioned previously, this paper focuses on applications where feedforward is the only or prominent mode of control. An alternative approach, therefore, is to improve the robustness of feedforward tracking controllers without relying on feedback, using a priori knowledge of plant uncertainty, e.g., Refs. [20] and [21]. Recently, motivated by use of a

¹ Corresponding author.

priori knowledge of plant uncertainty, optimal selection of coefficients [29] and optimal filtering of basis functions [30,31] have been explored as avenues to improve the robustness of the FBF approach. However, optimal selection of basis functions presents an opportunity for improving the robustness of the FBF approach that is unavailable to other feedforward tracking control methods; it could be used as an alternative or complement to existing methods. Recently, Ref. [32] has proposed an optimal set of basis functions to achieve a desired level of tracking accuracy with minimum control effort. The optimization was realized using the Frobenius norm of the lifted system representation (LSR) of the FBF's error as well as controller dynamics. In a similar vein as Ref. [32], this paper explores optimal basis function selection for robust tracking control using the FBF approach. This paper (and its preliminary version [33]) makes the following original contributions to the literature:

- It analyzes the effect of basis functions on the tracking accuracy of FBF, in the presence of uncertainty, using the Frobenius norm of the LSR of the error dynamics.
- (2) It proposes a process for optimally selecting basis functions to maximize the robustness of tracking control of uncertain linear systems using FBF.
- (3) It proposes an approach to ensure that the so-called "robust basis functions" resulting from the optimal selection process do not result in very large control inputs when applied to NMP systems.

The paper is structured as follows: Sec. 2 presents some background information on the FBF approach and the Frobenius norm metric and motivates the rest of the paper using an example. The contributions of the paper are presented in Sec. 3. Section 4 demonstrates the effectiveness of the proposed basis functions using a simulation example and experiments on a desktop 3D printer, and Sec. 5 concludes the paper.

2 Background and Motivation

2.1 Tracking Control Problem. For the sake of simplicity, the FBF approach is presented here in the context of a linear time invariant (LTI) single-input single-output (SISO) system. However, it is applicable to any discrete-time linear system [10,11,32]. Given a discrete-time LTI SISO system, G(q), as shown in Fig. 1, which may represent a stable open-loop plant or a stable closed-loop-controlled system, we can write

$$y(k) = G(q)u(k) \tag{1}$$

where k is the time index, q is the forward shift operator, and y and u are the output and control input, respectively. The objective of feedforward tracking control is to design a controller C(q) or find a control input u(k) given by

$$u(k) = C(q)y_d(k) \tag{2}$$

where $y_d(k)$ is the desired trajectory, such that the tracking error e(k)

$$e(k) = y_d(k) - y(k) = (1 - \underbrace{G(q)C(q)}_{L(q)})y_d(k) = E_{ff}(q)y_d(k)$$
(3)

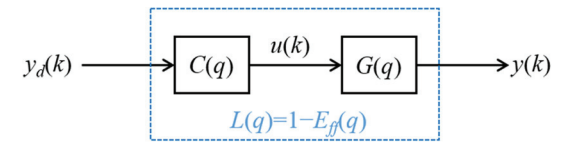


Fig. 1 Block diagram for feedforward tracking control

is minimized, where L(q) and $E_{\rm ff}(q)$ are the overall dynamics and the error dynamics of the controlled system, respectively.

For finite time, $0 \le k \le M$ (M+1 is the number of discrete points in the trajectory), the desired trajectory, control input, tracking error, and output trajectory can be expressed using vectors

$$\mathbf{y}_{d} = [y_{d}(0) \ y_{d}(1) \ \dots \ y_{d}(M)]^{\mathsf{T}}, \ \mathbf{u} = [u(0) \ u(1) \ \dots \ u(M)]^{\mathsf{T}}$$

$$\mathbf{e} = [e(0) \ e(1) \ \dots \ e(M)]^{\mathsf{T}}, \ \mathbf{y} = [y(0) \ y(1) \ \dots \ y(M)]^{\mathsf{T}}$$
(4)

Accordingly, Eqs. (1)–(3) can be expressed as

$$\mathbf{y} = \mathbf{G}\mathbf{u}; \quad \mathbf{u} = \mathbf{C}\mathbf{y}_d; \quad \mathbf{e} = (\mathbf{I} - \mathbf{L})\mathbf{y}_d = \mathbf{E}_{\mathrm{ff}}\mathbf{y}_d$$
 (5)

where G, C, L, and $E_{\rm ff}$ are the lifted system representations (see Appendix A for more details) of G, C, L, and $E_{\rm ff}$, respectively, and I is the identity matrix of appropriate size. The use of bold-face symbols for LSR of systems is maintained hereinafter.

2.2 Overview of the Filtered Basis Functions Approach. Here, we provide an overview of the FBF approach, assuming no uncertainty in the plant dynamics, to provide the reader with some background needed for the proposed approach including uncertainty discussed in Sec. 3. The FBF approach relies on two assumptions:

- (1) the desired trajectory is known a priori; and
- (2) the control input u(k) is expressed as a linear combination of n+1 user-defined basis functions $\varphi_i(k)$; i.e.,

$$u(k) = \sum_{i=0}^{n} \gamma_i \varphi_i(k) \tag{6}$$

where γ_i are unknown coefficients. Using vectors, Eq. (6) can be expressed as

$$\mathbf{u} = \mathbf{\Phi} \mathbf{\gamma}$$

$$\mathbf{\Phi} = [\mathbf{\varphi}_0 \quad \mathbf{\varphi}_1 \quad \dots \quad \mathbf{\varphi}_n], \ \mathbf{\varphi}_i = [\varphi_i(0) \quad \varphi_i(1) \quad \dots \quad \varphi_i(M)]^{\mathrm{T}},$$

$$\mathbf{\gamma} = [\gamma_0 \quad \gamma_1 \quad \dots \quad \gamma_n]^{\mathrm{T}}$$
(7)

Hence, for a linear system G(q), y can be expressed as

$$\begin{split} & \mathbf{y} = \tilde{\boldsymbol{\Phi}} \boldsymbol{\gamma} \\ & \tilde{\boldsymbol{\Phi}} = \mathbf{G}_{nom} \boldsymbol{\Phi}; \ \tilde{\boldsymbol{\phi}}_i = \mathbf{G}_{nom} \boldsymbol{\phi}_i; \ \tilde{\boldsymbol{\Phi}} = \begin{bmatrix} \tilde{\boldsymbol{\phi}}_0 & \tilde{\boldsymbol{\phi}}_1 & \dots & \tilde{\boldsymbol{\phi}}_n \end{bmatrix} \end{split}$$

where $\tilde{\Phi}$ represents the filtered basis functions matrix, i.e., Φ filtered through the LSR of a nominal model G_{nom} of the actual plant, as shown in Fig. 2. Note that, because in this section uncertainty in plant dynamics is not considered, $G_{nom} = G$ is assumed. The control objective is to find the optimal coefficient vector γ such that the squared two-norm of the tracking error

$$\mathbf{e}^{\mathrm{T}}\mathbf{e} = (\mathbf{y}_d - \tilde{\mathbf{\Phi}}\boldsymbol{\gamma})^{\mathrm{T}}(\mathbf{y}_d - \tilde{\mathbf{\Phi}}\boldsymbol{\gamma}) \tag{9}$$

is minimized; the optimal solution is given by

$$\mathbf{\gamma}^* = (\tilde{\mathbf{\Phi}}^{\mathrm{T}} \tilde{\mathbf{\Phi}})^{-1} \tilde{\mathbf{\Phi}}^{\mathrm{T}} \mathbf{y}_d \tag{10}$$

Based on Eqs. (5), (7), (8), and (10), the LSRs of the controller and error dynamics can be expressed as

$$\begin{aligned} C &= \Phi (\tilde{\Phi}^T \tilde{\Phi})^{-1} \tilde{\Phi}^T \\ E_{ff} &= I - \underbrace{\tilde{\Phi} (\tilde{\Phi}^T \tilde{\Phi})^{-1} \tilde{\Phi}^T}_{I} \end{aligned} \tag{11}$$

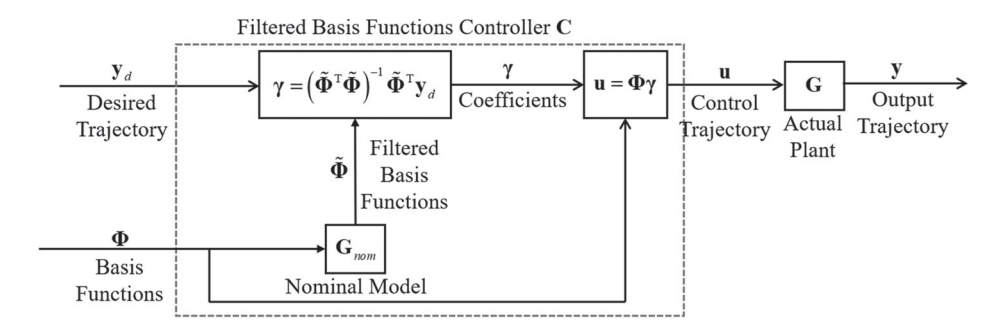


Fig. 2 Block diagram for feedforward tracking control using FBF approach

Remark 1. C and $E_{\rm ff}$ both depend on the system as well as the selected basis functions. Both matrices are, in general, non-Toeplitz and nontriangular implying that the FBF controller is, in general, LTV and noncausal [10].

Remark 2. The use of the LSR for formulating the FBF approach indicates its applicability to any discrete-time linear system (e.g., LTV or multi-input multi-output) because of their amenability to LSR.

2.3 Frobenius Norm Metric. As a tracking performance evaluation metric, the authors (in Refs. [15] and [32]) have proposed the following metric, J_e , based on the Frobenius norm of $\mathbf{E}_{\rm ff}$

$$J_e = \frac{\|\mathbf{E}_{\text{ff}}\|_F}{\sqrt{M+1}}; \quad \|\mathbf{E}_{\text{ff}}\|_F = \sqrt{\text{Tr}(\mathbf{E}_{\text{ff}}^T \mathbf{E}_{\text{ff}})} = \sqrt{\sum_i \left\{\sigma_i(\mathbf{E}_{\text{ff}})\right\}^2}$$
(12)

where Tr is the trace of a matrix. The Frobenius norm is selected because it takes into account all singular values/gains (σ_i) of \mathbf{E}_{ff} , as opposed to, e.g., $||\mathbf{E}_{\mathrm{ff}}||_2$, which considers only the maximum singular value/gain.

Note that for a normalized desired trajectory ($||\mathbf{y}_d||_2 = 1$)

$$\mathbf{e}_{\text{RMS}} = \frac{||\mathbf{e}||_2}{\sqrt{M+1}} \le \frac{||\mathbf{E}_{\text{ff}}||_F}{\sqrt{M+1}} = J_e$$
 (13)

The implication is that J_e is an upper bound on the root-mean-square (RMS) tracking error (e_{RMS}). Moreover, it is shown in Ref. [32], that for an LTI system

$$\frac{\|\mathbf{E}_{\mathrm{ff}}\|_{F}}{\sqrt{M+1}} \to \|E_{\mathrm{ff}}(q)\|_{2} \quad \text{as} \quad M \to \infty$$
 (14)

In other words, J_e approaches the system error two-norm criterion (sometimes used in the design and analysis of LTI tracking controllers [34]).

2.4 Motivational Example. This section motivates the rest of the paper, using a damped oscillator with parametric uncertainty

$$G(s) = \frac{\omega_n^2}{s^2 + 2\zeta\omega_n s + \omega_n^2}$$

$$\omega_{n,\text{nom}} = 200 \,\text{Hz}, \ \zeta_{\text{nom}} = 0.01$$

$$\omega_n \in \begin{bmatrix} 180, & 220 \end{bmatrix} \,\text{Hz}, \ \zeta \in \begin{bmatrix} 0.001, & 0.1 \end{bmatrix}$$
(15)

where ω_n and ζ denote the natural frequency and damping ratio, and the subscript "nom" denotes the nominal value. The system in Eq. (15) is representative of the dynamics of a vibration-prone 3D printer with uncertainty [12,30] (also shown in Fig. 9). The system

is sampled at 1 kHz. The set of actual plant dynamics is generated by selecting 410 evenly distributed realizations of the plant defined by Eq. (15). The nominal values of the plant parameters are used to generate the nominal model for filtering the basis functions. The desired signal \mathbf{y}_d is a white noise signal with zero mean and unit variance (M = 1000). The choice of white noise for \mathbf{y}_d is because its broadband nature eliminates biased results based on arbitrarily selected \mathbf{y}_d . There is a wide choice of basis functions that can be used with the FBF approach. This work uses discrete cosine transform (DCT) [28], block pulse functions (BPF) [35], and B-splines [36], due to their popularity (Appendix B gives more details about each basis function).

Figure 3 shows the normalized RMS tracking error $\mathbf{e}_{\text{RMS}}/\mathbf{y}_{d,\text{RMS}}$ for DCT, BPF, and B-splines, for various numbers of basis functions (n=10–990), using the 410 realizations of the actual plant dynamics G, described previously. The metrics used for comparison are the mean, standard deviation, and nominal values (assuming the plant model is perfect) of $\mathbf{e}_{\text{RMS}}/\mathbf{y}_{d,\text{RMS}}$. It is observed that for the same n, the nominal tracking accuracy of FBF does not vary significantly with the type of basis functions. This observation is in agreement with the discussion in prior work [32]. However, it is observed that the tracking accuracy of the FBF approach deteriorates in the presence of uncertainty and varies significantly depending on the type of basis functions. Hence, a methodology for selecting an optimal set of basis functions for robust tracking control using FBF is needed.

3 Optimal Selection of Basis Functions for Robust Tracking

In this section, we propose an optimization process for selection of basis functions for robust tracking. First, we reformulate the FBF approach discussed in Sec. 2.1 to include uncertainty. Next,

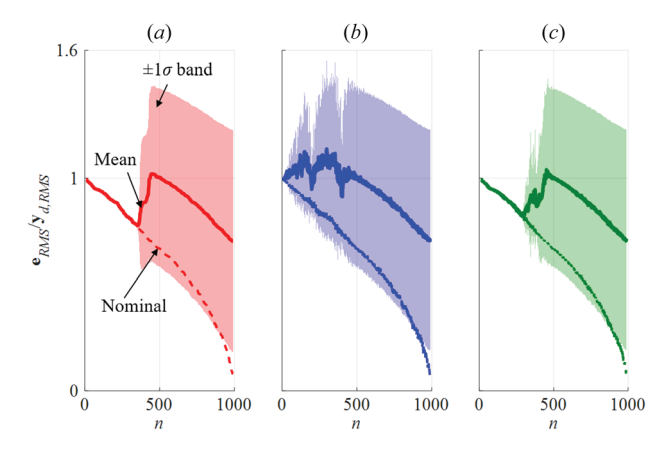


Fig. 3 Comparison of normalized RMS tracking error for DCT, BPF, and B-splines, in the absence (nominal) and presence of uncertainty, as functions of number of basis functions

we analyze the effect of uncertainty and basis functions on the tracking accuracy of the FBF approach, using the Frobenius norm metric, then we find a set of robust basis functions that minimize the effect of the uncertainty. Finally, to avoid large control inputs for NMP systems, an approach to constrain the control input while selecting the robust basis functions is presented.

3.1 Effect of Uncertainty and Basis Functions on Tracking Accuracy of the Filtered Basis Functions Approach. Referring to Fig. 2, assume that, due to uncertainty, the LSR of actual plant dynamics **G** belongs to the set $\{\mathbf{G}_{aj}\}$, j=1,2,...,l. The set could represent a plant with additive uncertainty, multiplicative uncertainty, parametric uncertainty, etc. Without loss of generality, this paper assumes that the set has a finite number of members which sufficiently sample the uncertainty. Sampling of uncertainty has been used in the literature, e.g., Refs. [21] and [37], for robust controller design. Also, because of uncertainty, the nominal model \mathbf{G}_{nom} used to design the FBF controller (see Fig. 2) is not necessarily equal to \mathbf{G} and may or may not belong to the set $\{\mathbf{G}_{aj}\}$. Accordingly, the LSR of the error dynamics corresponding to \mathbf{G}_{aj} is given by \mathbf{E}_{fij} . To analyze the robustness of \mathbf{C} , the Frobenius norm metric $J_{e,r}$ can be expressed as

$$J_{e,r}^{2} = \sum_{j=1}^{l} \lambda_{j} J_{ej}^{2}; \quad J_{ej} = \frac{\|\mathbf{E}_{ffj}\|_{F}}{\sqrt{M+1}} = \frac{\|\mathbf{I} - \mathbf{G}_{aj}\mathbf{C}\|_{F}}{\sqrt{M+1}}; \quad \sum_{j=1}^{l} \lambda_{j} = 1$$
(16)

where $\{\lambda_j\}$ denotes weights associated with the distribution of the uncertainty. Note that G_{nom} may or may not belong to $\{G_{aj}\}$.

Remark 3. Note that the metric given by Eq. (16) is based on summation over the entire set of uncertain plant dynamics $\{G_{aj}\}$, as opposed to the worst-case G_{aj} . Worst-case plant dynamics is often considered in robust feedback control, due to the need to guarantee stability based on the worst-case scenario. However, in feedforward tracking control where tracking accuracy is of primary interest, a worst-case design tends to be overly conservative, especially if the worst-case rarely occurs in practice [21]. Hence, an approach which considers the distribution of the occurrence of the uncertain plant dynamics is considered in this paper.

Remark 4. This paper focuses on FBF, and hence the metric $J_{e,r}$ will only be explored in the context of FBF in the remainder of this paper. However, the metric can be used to analyze robustness of other tracking controllers.

If C is designed using G_{nom} , then C is given by

$$\mathbf{C} = \mathbf{\Phi}(\tilde{\mathbf{\Phi}}^{\mathrm{T}}\tilde{\mathbf{\Phi}})^{-1}\tilde{\mathbf{\Phi}}^{\mathrm{T}} \tag{17}$$

Since analysis using the pseudoinverse is quite cumbersome, $\tilde{\Phi} = G_{nom}\Phi$ is transformed into the decoupled filtered basis functions matrix $\tilde{\Psi} = G_{nom}\Psi$ [10]. After transformation, C and E_{ffj} can be expressed as

$$\mathbf{C} = \mathbf{\Psi}\tilde{\mathbf{\Psi}}^{\mathrm{T}}; \quad \mathbf{E}_{\mathrm{ff}j} = \mathbf{I}_{M+1} - \tilde{\mathbf{\Psi}}_{aj}\tilde{\mathbf{\Psi}}^{\mathrm{T}}; \quad \tilde{\mathbf{\Psi}}^{\mathrm{T}}\tilde{\mathbf{\Psi}} = \mathbf{I}_{n+1}$$
 (18)

where $\tilde{\Psi}_{aj}$ is obtained by filtering $\tilde{\Psi}$ using G_{aj} .

Proposition 1. For the set $\{G_{aj}\}$ and associated weights $\{\lambda_j\}$, $J_{e,r}$ can be expressed in terms of the uncertainty and basis functions as

$$J_{e,r}^2 = 1 - \frac{n+1}{M+1} + \sum_{j=1}^{l} \lambda_j \frac{\|(\mathbf{G}_{aj} - \mathbf{G}_{\text{nom}})\mathbf{\Psi}\|_F^2}{M+1}$$
(19)

Proof. This proof first finds the metric J_{ej} and then finds $J_{e,r}$ using Eq. (16). Based on Eqs. (16) and (18)

$$\begin{split} \|\mathbf{E}_{ffj}\|_{F}^{2} &= \mathrm{Tr}(\mathbf{E}_{ffj}^{\mathrm{T}}\mathbf{E}_{ffj}) = \mathrm{Tr}((\mathbf{I}_{M+1} - \tilde{\mathbf{\Psi}}_{aj}\tilde{\mathbf{\Psi}}^{\mathrm{T}})^{\mathrm{T}}(\mathbf{I}_{M+1} - \tilde{\mathbf{\Psi}}_{aj}\tilde{\mathbf{\Psi}}^{\mathrm{T}})) \\ &= \mathrm{Tr}(\mathbf{I}_{M+1} - \tilde{\mathbf{\Psi}}_{aj}\tilde{\mathbf{\Psi}}^{\mathrm{T}} - \tilde{\mathbf{\Psi}}\tilde{\mathbf{\Psi}}_{aj}^{\mathrm{T}} + \tilde{\mathbf{\Psi}}\tilde{\mathbf{\Psi}}_{aj}^{\mathrm{T}}\tilde{\mathbf{\Psi}}_{aj}\tilde{\mathbf{\Psi}}^{\mathrm{T}}) \\ &= \mathrm{Tr} \begin{pmatrix} \mathbf{I}_{M+1} - \{\tilde{\mathbf{\Psi}} + \delta\tilde{\mathbf{\Psi}}_{aj}\}\tilde{\mathbf{\Psi}}^{\mathrm{T}} - \tilde{\mathbf{\Psi}}\{\tilde{\mathbf{\Psi}} + \delta\tilde{\mathbf{\Psi}}_{aj}\}^{\mathrm{T}} \\ \\ &+ \tilde{\mathbf{\Psi}}\{\tilde{\mathbf{\Psi}} + \delta\tilde{\mathbf{\Psi}}_{aj}\}^{\mathrm{T}}\{\tilde{\mathbf{\Psi}} + \delta\tilde{\mathbf{\Psi}}_{aj}\}\tilde{\mathbf{\Psi}}^{\mathrm{T}} \end{pmatrix} \\ \delta\tilde{\mathbf{\Psi}}_{aj} \triangleq \tilde{\mathbf{\Psi}}_{aj} - \tilde{\mathbf{\Psi}} \end{split} \tag{20}$$

Using the fact that trace is a linear mapping and is invariant under cyclic permutations

$$\|\mathbf{E}_{ffj}\|_{F}^{2} = \underbrace{\operatorname{Tr}(\mathbf{I}_{M+1})}_{=M+1} - \underbrace{\operatorname{Tr}(\tilde{\mathbf{\Psi}}\tilde{\mathbf{\Psi}}^{T})}_{=n+1} - \operatorname{Tr}(\delta\tilde{\mathbf{\Psi}}_{aj}\tilde{\mathbf{\Psi}}^{T}) - \underbrace{\operatorname{Tr}(\tilde{\mathbf{\Psi}}\tilde{\mathbf{\Psi}}^{T})}_{=n+1} - \underbrace{\operatorname{Tr}(\tilde{\mathbf{\Psi}}\delta\tilde{\mathbf{\Psi}}_{aj}^{T})}_{=n+1} + \underbrace{\operatorname{Tr}(\tilde{\mathbf{\Psi}}\delta\tilde{\mathbf{\Psi}}_{aj}^{T}\tilde{\mathbf{\Psi}}\tilde{\mathbf{\Psi}}^{T})}_{=\operatorname{Tr}(\tilde{\mathbf{\Psi}}\delta\tilde{\mathbf{\Psi}}_{aj}^{T})} + \underbrace{\operatorname{Tr}(\tilde{\mathbf{\Psi}}\tilde{\mathbf{\Psi}}^{T}\delta\tilde{\mathbf{\Psi}}_{aj}\tilde{\mathbf{\Psi}}^{T})}_{=\operatorname{Tr}(\delta\tilde{\mathbf{\Psi}}_{aj}\tilde{\mathbf{\Psi}}^{T})} + \underbrace{\operatorname{Tr}(\tilde{\mathbf{\Psi}}\delta\tilde{\mathbf{\Psi}}_{aj}^{T}\delta\tilde{\mathbf{\Psi}}_{aj}\tilde{\mathbf{\Psi}}^{T})}_{=\|\delta\tilde{\mathbf{\Psi}}_{aj}\|_{F}^{2}} = (M+1) - (n+1) + \|\delta\tilde{\mathbf{\Psi}}_{aj}\|_{F}^{2}$$

$$(21)$$

Substituting Eq. (21) in Eq. (16) gives

$$J_{e,r}^{2} = \sum_{j=1}^{l} \lambda_{j} J_{ej}^{2} = 1 - \frac{n+1}{M+1} + \sum_{j=1}^{l} \lambda_{j} \frac{\|(\mathbf{G}_{aj} - \mathbf{G}_{\text{nom}})\mathbf{\Psi}\|_{F}^{2}}{M+1}$$
 (22)

Remark 5. The metric can be expressed as

$$J_{e,r}^{2} = J_{e,\text{nom}}^{2} + J_{e,\text{unc}}^{2}; \quad J_{e,\text{nom}}^{2} \triangleq 1 - \frac{n+1}{M+1};$$

$$J_{e,\text{unc}}^{2} \triangleq \sum_{i=1}^{l} \lambda_{ij} \frac{\|(\mathbf{G}_{aj} - \mathbf{G}_{\text{nom}})\mathbf{\Psi}\|_{F}^{2}}{M+1}$$
(23)

The implication is that the metric is the summation of two components—nominal and uncertainty-related. The nominal component is identical to the value of the metric in the absence of the uncertainty [32]; it only depends on the number of basis functions and is independent of the plant dynamics and the choice of basis functions. However, the uncertainty-related component depends on the uncertainty, choice of nominal model, and the type and number of basis functions. With increase in n, the nominal component decreases monotonically, whereas, due to the Frobenius norm, the uncertainty-related component generally increases with n. The implication is that the tracking error for FBF in the presence of uncertainty does not vary monotonically with the number of basis functions (as seen in Fig. 3).

3.2 Proposed Approach for Optimal Selection of Basis Functions. In this section, we find an optimal set of basis functions that minimizes $J_{e,r}$ for a given nominal model G_{nom} and actual plant $\{G_{aj}\}$. Toward achieving this objective, we first find an optimal set of basis functions that minimize the uncertainty-related component of $J_{e,\text{unc}}$, for a given value of $J_{e,\text{nom}}$. The

procedure for selection of optimal basis functions is outlined in Proposition 2.

Proposition 2. Given $\{G_{aj}\}$, $\{\lambda_j\}$, and G_{nom} , the n+1 basis functions Ψ that minimize $J_{e,unc}$ are given by

$$\begin{split} \mathbf{\Psi} &= \mathbf{W}_{\text{nom}} \mathbf{\Sigma}_{\text{nom}}^{-1} \mathbf{W}_{\bar{\mathbf{\Delta}}_{\text{nom}}} \begin{bmatrix} \mathbf{0}_{(M-n) \times (n+1)} \\ \mathbf{I}_{n+1} \end{bmatrix} \\ \mathbf{G}_{\text{nom}} &= \mathbf{V}_{\text{nom}} \mathbf{\Sigma}_{\text{nom}} \mathbf{W}_{\text{nom}}^{\text{T}}; \quad \bar{\mathbf{\Delta}}_{\text{nom}} &= \mathbf{V}_{\bar{\mathbf{\Delta}}_{\text{nom}}} \mathbf{\Sigma}_{\bar{\mathbf{\Delta}}_{\text{nom}}} \mathbf{W}_{\bar{\mathbf{\Delta}}_{\text{nom}}}^{\text{T}} \\ \bar{\mathbf{\Delta}}_{\text{nom}} &= \mathbf{\Delta} \mathbf{W}_{\text{nom}} \mathbf{\Sigma}_{\text{nom}}^{-1}; \quad \mathbf{\Delta}^{\text{T}} \mathbf{\Delta} &= \sum_{j=1}^{l} \lambda_{j} (\mathbf{G}_{aj} - \mathbf{G}_{\text{nom}})^{\text{T}} (\mathbf{G}_{aj} - \mathbf{G}_{\text{nom}}) \end{split}$$

$$(24)$$

where V_{nom} , Σ_{nom} , and W_{nom} denote the left singular vector matrix, singular value matrix, and right singular vector matrix of G_{nom} , respectively. Similarly, $V_{\bar{\Lambda}_{nom}}$, $\Sigma_{\bar{\Lambda}_{nom}}$, and $W_{\bar{\Lambda}_{nom}}$ denote the left singular vector matrix, singular value matrix, and right singular vector matrix of $\bar{\Lambda}_{nom}$, respectively.

Proof. The problem of minimizing $J_{e,\text{unc}}$ for a given value of n can be expressed using Eq. (23) as

$$\min_{\mathbf{\Psi}} \left[J_{e,\text{unc}}^2 = \sum_{j=1}^l \lambda_j \frac{\|(\mathbf{G}_{aj} - \mathbf{G}_{\text{nom}})\mathbf{\Psi}\|_F^2}{M+1} \right]$$
subject to $\tilde{\mathbf{\Psi}}^{\text{T}} \tilde{\mathbf{\Psi}} = \mathbf{I}_{n+1}$ (25)

Note that the constraint is a result of the decoupling process (Eq. (18)). The objective of the problem, given by Eq. (25), can alternatively be expressed as

$$J_{e,\text{unc}}^{2} = \sum_{i=1}^{l} \lambda_{j} \frac{\|(\mathbf{G}_{aj} - \mathbf{G}_{\text{nom}})\mathbf{\Psi}\|_{F}^{2}}{M+1} = \frac{\text{Tr}(\mathbf{\Psi}^{T} \mathbf{\Delta}^{T} \mathbf{\Delta} \mathbf{\Psi})}{M+1}$$
(26)

Equation (26) can be expressed as

$$J_{e,\text{unc}}^{2} = \frac{\|\Delta\Psi\|_{F}^{2}}{M+1} = \frac{\|\Delta\mathbf{G}_{\text{nom}}^{-1}\tilde{\Psi}\|_{F}^{2}}{M+1} = \frac{\|\Delta\mathbf{W}_{\text{nom}}\boldsymbol{\Sigma}_{\text{nom}}^{-1}\mathbf{V}_{\text{nom}}^{T}\tilde{\Psi}\|_{F}^{2}}{M+1}$$
$$= \frac{\|\bar{\Delta}_{\text{nom}}\tilde{\boldsymbol{\Xi}}\|_{F}^{2}}{M+1}$$
(27)

$$\bar{\boldsymbol{\Delta}}_{nom} \triangleq \boldsymbol{\Delta} \boldsymbol{W}_{nom} \boldsymbol{\Sigma}_{nom}^{-1}; \; \tilde{\boldsymbol{\Xi}} \triangleq \boldsymbol{V}_{nom}^T \tilde{\boldsymbol{\Psi}}$$

The constraint in Eq. (25) can be expressed as

$$\tilde{\boldsymbol{\Psi}}^{\mathrm{T}}\tilde{\boldsymbol{\Psi}} = \mathbf{I}_{n+1} \Rightarrow \tilde{\boldsymbol{\Psi}}^{\mathrm{T}}\mathbf{V}_{\mathrm{nom}}\mathbf{V}_{\mathrm{nom}}^{\mathrm{T}}\tilde{\boldsymbol{\Psi}} = \mathbf{I}_{n+1} \Rightarrow \tilde{\boldsymbol{\Xi}}^{\mathrm{T}}\tilde{\boldsymbol{\Xi}} = \mathbf{I}_{n+1} \quad (28)$$

Hence, the optimization problem given by Eq. (25) can be rewritten as

$$\min_{\tilde{\mathbf{\Xi}}} \left[J_{e,\text{unc}}^2 = \frac{\|\bar{\mathbf{\Delta}}_{\text{nom}}\tilde{\mathbf{\Xi}}\|_F^2}{M+1} \right]$$
(29)

subject to
$$\tilde{\Xi}^{\mathrm{T}}\tilde{\Xi} = \mathbf{I}_{n+1}$$

The optimal basis functions for robustness are the set of right singular vectors of the matrix $\bar{\mathbf{\Delta}}_{nom}$, corresponding to its n+1 smallest singular values [32], i.e.,

$$\tilde{\mathbf{\Xi}} = \mathbf{W}_{\bar{\mathbf{\Delta}}_{\text{nom}}} \begin{bmatrix} \mathbf{0}_{(M-n)\times(n+1)} \\ \mathbf{I}_{n+1} \end{bmatrix}; \ \bar{\mathbf{\Delta}}_{\text{nom}} = \mathbf{V}_{\bar{\mathbf{\Delta}}_{\text{nom}}} \mathbf{\Sigma}_{\bar{\mathbf{\Delta}}_{\text{nom}}} \mathbf{W}_{\bar{\mathbf{\Delta}}_{\text{nom}}}^{\mathbf{T}}$$
(30)

and the corresponding basis functions are

$$\Psi = \mathbf{W}_{\text{nom}} \mathbf{\Sigma}_{\text{nom}}^{-1} \mathbf{V}_{\text{nom}}^{\text{T}} \tilde{\mathbf{\Psi}} = \mathbf{W}_{\text{nom}} \mathbf{\Sigma}_{\text{nom}}^{-1} \tilde{\mathbf{\Xi}}$$

$$= \mathbf{W}_{\text{nom}} \mathbf{\Sigma}_{\text{nom}}^{-1} \mathbf{W}_{\tilde{\mathbf{\Delta}}_{\text{nom}}} \begin{bmatrix} \mathbf{0}_{(M-n) \times (n+1)} \\ \mathbf{I}_{n+1} \end{bmatrix}$$
(31)

3.3 Constraining Control Effort for Nonminimum Phase Systems. Although the basis functions obtained by Eq. (31) are optimal in terms of robustness, they might result in large control inputs, especially if G_{nom} has very small singular values. Very small singular values might result in an unrealizable robust controller [32], and hence the optimal basis functions should be designed to avoid components corresponding to these very small singular values.

Proposition 3. Given $\{G_{aj}\}$, $\{\lambda_j\}$, and G_{nom} (with r very small singular values, due to NMP zeros or nonzero relative degree [32]), the n+1 basis functions Ψ that minimize $J_{e,unc}$ while avoiding the very small singular values of G_{nom} are given by

$$\Psi = \mathbf{W}_{\text{nom}} \mathbf{\Sigma}_{\text{nom}}^{-1} \begin{bmatrix} \mathbf{W}_{\bar{\mathbf{\Delta}}_{\text{nom},s}} \begin{bmatrix} \mathbf{0}_{(M-n-r)\times(n+1)} \\ \mathbf{I}_{n+1} \end{bmatrix} \end{bmatrix}$$

$$\mathbf{G}_{\text{nom}} = \mathbf{V}_{\text{nom}} \mathbf{\Sigma}_{\text{nom}} \mathbf{W}_{\text{nom}}^{\text{T}}; \quad \bar{\mathbf{\Delta}}_{\text{nom},s} = \mathbf{V}_{\bar{\mathbf{\Delta}}_{\text{nom},s}} \mathbf{\Sigma}_{\bar{\mathbf{\Delta}}_{\text{nom},s}} \mathbf{W}_{\bar{\mathbf{\Delta}}_{\text{nom},s}}^{\text{T}}$$

$$\bar{\mathbf{\Delta}}_{\text{nom}} = \mathbf{\Delta} \mathbf{W}_{\text{nom}} \mathbf{\Sigma}_{\text{nom}}^{-1} = [\bar{\mathbf{\Delta}}_{\text{nom},s} \quad \bar{\mathbf{\Delta}}_{\text{nom},r}];$$

$$\mathbf{\Delta}^{\text{T}} \mathbf{\Delta} = \sum_{i}^{l} \lambda_{j} (\mathbf{G}_{aj} - \mathbf{G}_{\text{nom}})^{\text{T}} (\mathbf{G}_{aj} - \mathbf{G}_{\text{nom}})$$

$$(32)$$

(26) where V_{nom} , Σ_{nom} , W_{nom} , $V_{\bar{\Lambda}_{nom,s}}$, $\Sigma_{\bar{\Lambda}_{nom,s}}$, and $W_{\bar{\Lambda}_{nom,s}}$ are defined in Eq. (24). Also, $\bar{\Lambda}_{nom,s}$ and $\bar{\Lambda}_{nom,r}$ are the first M+1-r columns and last r columns of $\bar{\Lambda}_{nom}$, respectively.

Proof. Based on the discussion in Ref. [32], the components corresponding to r very small singular values of \mathbf{G}_{nom} can be avoided by equating the elements of last r rows of $\tilde{\Xi}_{nom}$ to zero, i.e., reformulate Eq. (29) as

$$\min_{\tilde{\Xi}} \left[J_{e,\text{unc}}^2 = \frac{\|\bar{\mathbf{\Delta}}_{\text{nom}}\tilde{\mathbf{\Xi}}\|_F^2}{M+1} \right] \\
\text{subject to } \tilde{\mathbf{\Xi}}^T \tilde{\mathbf{\Xi}} = \mathbf{I}_{n+1} \tag{33}$$

the last r rows of $\tilde{\Xi}$ have elements equal to 0

The new constraint can be embedded into the objective and orthogonality constraint by

$$\bar{\mathbf{\Delta}}_{\text{nom}}\tilde{\mathbf{\Xi}} = \begin{bmatrix} \bar{\mathbf{\Delta}}_{\text{nom},s} & \bar{\mathbf{\Delta}}_{\text{nom},r} \end{bmatrix} \begin{bmatrix} \tilde{\mathbf{\Xi}}_{s} \\ \mathbf{0}_{r \times (n+1)} \end{bmatrix} = \bar{\mathbf{\Delta}}_{\text{nom},s}\tilde{\mathbf{\Xi}}_{s}$$

$$\tilde{\mathbf{\Xi}}^{T}\tilde{\mathbf{\Xi}} = \begin{bmatrix} \tilde{\mathbf{\Xi}}_{s}^{T} & \mathbf{0}_{(n+1) \times r} \end{bmatrix} \begin{bmatrix} \tilde{\mathbf{\Xi}}_{s} \\ \mathbf{0}_{r \times (n+1)} \end{bmatrix} = \tilde{\mathbf{\Xi}}_{s}^{T}\tilde{\mathbf{\Xi}}_{s}$$
(34)

where $\bar{\Delta}_{\text{nom},r}$ and $\bar{\Delta}_{\text{nom},r}$ are defined in Eq. (32). The optimization problem, given by Eq. (33), can be rewritten as

$$\min_{\tilde{\Xi}_{s}} \|\bar{\Delta}_{\text{nom},s}\tilde{\Xi}_{s}\|_{F}^{2}$$
s.t. $\tilde{\Xi}_{s}^{T}\tilde{\Xi}_{s} = \mathbf{I}_{n+1}$
(35)

The optimal solution to Eq. (35) is the set of right singular vectors of the matrix $\bar{\Delta}_{\text{nom},s}$ corresponding to its n+1 smallest singular values [32]

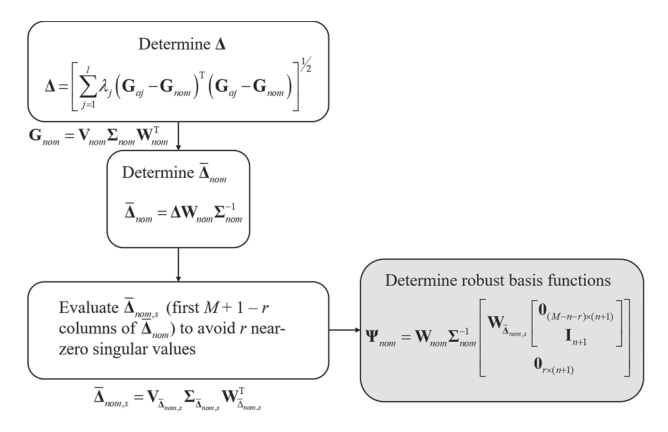


Fig. 4 Flowchart describing the process for optimal selection of robust basis functions to minimize $J_{e,\mathrm{nom}}$ while maintaining $J_{e,\mathrm{nom}}$ (i.e., minimize uncertainty while maintaining nominal tracking accuracy) and avoiding small singular values

$$\tilde{\mathbf{\Xi}}_{s} = \mathbf{W}_{\bar{\mathbf{\Delta}}_{\text{nom,s}}} \begin{bmatrix} \mathbf{0}_{(M-n-r)\times(n+1)} \\ \mathbf{I}_{n+1} \end{bmatrix}$$

$$\bar{\mathbf{\Delta}}_{\text{nom,s}} = \mathbf{V}_{\bar{\mathbf{\Delta}}_{\text{nom,s}}} \mathbf{\Sigma}_{\bar{\mathbf{\Delta}}_{\text{nom,s}}} \mathbf{W}_{\bar{\mathbf{\Delta}}_{\text{nom,s}}}^{T}$$
(36)

and the corresponding basis functions are

$$\Psi = \mathbf{W}_{\text{nom}} \mathbf{\Sigma}_{\text{nom}}^{-1} \mathbf{V}_{\text{nom}}^{\text{T}} \tilde{\mathbf{\Psi}}_{\text{nom}} = \mathbf{W}_{\text{nom}} \mathbf{\Sigma}_{\text{nom}}^{-1} \tilde{\mathbf{\Xi}}$$

$$= \mathbf{W}_{\text{nom}} \mathbf{\Sigma}_{\text{nom}}^{-1} \begin{bmatrix} \tilde{\mathbf{\Xi}}_{s} \\ \mathbf{0}_{r \times (n+1)} \end{bmatrix} = \mathbf{W}_{\text{nom}} \mathbf{\Sigma}_{\text{nom}}^{-1} \begin{bmatrix} \mathbf{W}_{\tilde{\mathbf{A}}_{\text{nom},s}} \begin{bmatrix} \mathbf{0}_{(M-n-r) \times (n+1)} \\ \mathbf{I}_{n+1} \end{bmatrix} \\ \mathbf{0}_{r \times (n+1)} \end{bmatrix}$$
(37)

Figure 4 summarizes the procedure for selection of optimal basis functions, described in Propositions 2 and 3.

Remark 6. Avoiding the very small singular values might have small adverse impact on the tracking accuracy but is largely beneficial in terms of minimizing the control input. In practice, the impact on tracking error would be very small because of the exponential/oscillatory nature of the singular vectors corresponding to the very small singular values, and their resulting small contribution to desired trajectories used in engineering applications. Also, inclusion of the very small singular values in selection of basis functions results in a very large control input to compensate for a small tracking error which can be easily addressed by avoiding the very small singular values.

Remark 7. Since the choice of basis functions only affects the uncertainty-related component and does not affect the nominal component (Remark 5), the proposed robust basis functions are selected such that robust tracking is realized without affecting the nominal tracking accuracy of FBF (Proposition 2). This is unlike other robust tracking controllers in the literature, e.g., Ref. [31], whose improved robustness in tracking is achieved at the cost of deterioration in nominal tracking accuracy.

Remark 8. For the basis functions given by Eq. (37), the value of metric $J_{e,\mathrm{unc}}$ is given by

$$J_{e,\text{unc}}^{2} = \frac{\sum_{i=M-r-n+1}^{M+1-r} \sigma_{\bar{\Lambda}_{\text{nom},s},i}^{2}}{M+1}$$
 (38)

where $\{\sigma_{\bar{\Lambda}_{nom,s},i}\}$, i=1, 2, ..., M+1-r are the singular values of the matrix $\bar{\Lambda}_{nom,s}$ in the descending order. For n=0 (1 basis

function), $J_{e, \text{unc}}$ only depends on the smallest singular value of $\bar{\Delta}_{\text{nom,s}}$. The implication is that in an M+1 dimensional vector space, the basis function is aligned with the most robust vector, i.e., the vector that ensures that the uncertainty has the least effect on the tracking accuracy of FBF. As n increases, new basis functions are added such that the next higher singular values are added to $J_{e, \text{unc}}$ and the next most robust vectors in the M+1 dimensional vector space are selected. Among all possible n+1 dimensional vector spaces for vectors of length M+1, the effect of the uncertainty on tracking accuracy of the FBF approach is minimum in the vector space created by the n+1 basis functions given by Eq. (37).

The value of $J_{e,r}$ for the proposed robust basis functions is given by

$$J_{e,r}^{2} = \underbrace{1 - \frac{n+1}{M+1}}_{J^{2}} + \underbrace{\frac{\sum\limits_{i=M-r-n+1}^{M+1-r} \sigma_{\bar{\Lambda}_{\text{nom},s},i}^{2}}{M+1}}_{J^{2}}$$
(39)

The difference in values of $J_{e,r}^2$ as n increases from $n = n_i$ to $n = n_i + 1$ is given by

$$J_{e,r}^{2}[n_{i}+1] - J_{e,r}^{2}[n_{i}] = \frac{\sigma_{\bar{\Lambda}_{\text{nom},s},M-r-n_{i}}^{2}}{M+1}$$
 (40)

where $J_{e,r}^2[n_i]$ denotes the value of $J_{e,r}^2$ for $n=n_i$. Hence, the value of the metric decreases (i.e., tracking accuracy improves) if $\sigma_{\bar{\Lambda}_{\text{nom},s},M-r-n_i} < 1$ and increases (i.e., tracking accuracy deteriorates) if $\sigma_{\bar{\Lambda}_{\text{nom},s},M-r-n_i} > 1$.

Remark 9. Based on the above discussion, following three scenarios are possible with the proposed optimal basis functions:

- (i) If all singular values $\{\sigma_{\bar{\Lambda}_{nom,s},l}\}$ are less than 1, then $J_{e,r}^2$ is a decreasing function of n. Thus, n=M-r results in the most robust basis functions for the given nominal model and actual plant.
- (ii) If all singular values $\{\sigma_{\bar{\Lambda}_{nom,s},i}\}$ are greater than 1, then $J_{e,r}^2$ is an increasing function of n, and n=0 results in the most robust basis functions for the given nominal model and actual plant.
- (iii) If $\{\sigma_{\bar{\Lambda}_{nom,s},i}\}$ has values dispersed on either side of 1, then for lower values of n, $J_{e,r}^2$ is a decreasing function of n, until $\sigma_{\bar{\Lambda}_{nom,s},M+1-r-n} < 1$, and for higher values of n, $J_{e,r}^2$ is an increasing function of n. The most robust basis functions, for the given nominal model and actual plant, are achieved at the highest value of n for which $\sigma_{\bar{\Lambda}_{nom,s},M+1-r-n} < 1$.

For a given uncertainty, scenario (i) would be the most desirable, since the optimal value is achieved for highest value of n (the most optimal nominal tracking accuracy and spans the entire possible trajectory space). This analysis also demonstrates that smaller singular values $\{\sigma_{\bar{\Lambda}_{nom,s},i}\}$ are desirable. Remark 10. Since the singular values depend on the uncertainty

Remark 10. Since the singular values depend on the uncertainty and the nominal model, an ideal way to optimize tracking accuracy of FBF, in addition to optimal selection of basis functions, would be to optimize the nominal model to minimize singular values of $\bar{\Delta}_{\text{nom,s}}$. The ongoing work of the authors [31,38] focuses on optimal selection of the nominal model for robust control.

4 Examples

4.1 Simulations. The discussion in this paper was motivated using a simple example in Sec. 2.4, and this section continues with the same example. The robust basis functions proposed in Sec. 3.3 are compared with popular basis functions in the literature, viz., DCT, BPF, and B-splines. While DCT, BPF, and B-splines are defined independent of the plant dynamics (see

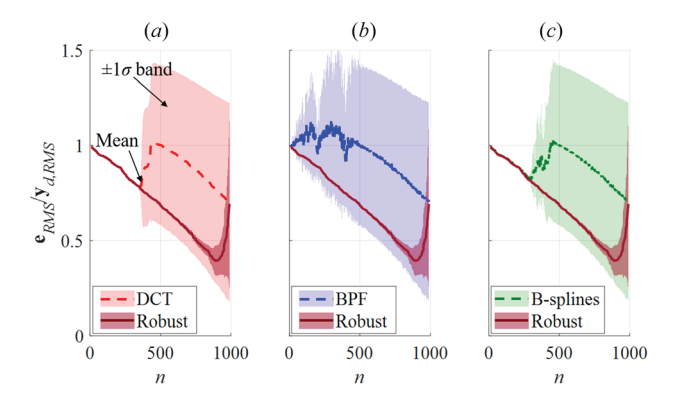


Fig. 5 Comparison of normalized RMS tracking error for DCT, BPF, B-splines, and the robust basis functions, in the presence of uncertainty, for various values of number of basis functions, n

Appendix B), the robust basis functions are designed based on the nominal model as well as the known uncertainty in the plant dynamics, using Proposition 3. The system and desired trajectory parameters are same as that in Sec. 2.4. For design of the robust basis functions, the set of possible actual plant dynamics $\{G_{aj}\}$ is generated by selecting l=410 evenly distributed realizations of the plant defined by Eq. (15) such that $\lambda_j=1/l$. Also, the LSRs of members of the set of possible actual plant dynamics $\{G_{aj}\}$ have one very small singular value, and hence r=1.

Figure 5 shows the normalized RMS tracking error $e_{RMS}/y_{d,RMS}$ for DCT, BPF, B-splines, and the proposed robust basis functions, for various numbers of basis functions (n = 10-990). The metrics used for comparison are the mean and standard deviation of $e_{RMS}/y_{d,RMS}$. It is observed that for all values of n, the robust basis functions result in minimum values of mean and standard deviation. For example, at n = 500, compared to DCT, BPF, and B-splines, the robust basis functions result in improvements in mean and standard deviations of $e_{RMS}/y_{d,RMS}$ by up to 1.5 times and 77 times, respectively. The nominal values of $e_{RMS}/y_{d,RMS}$ for DCT, BPF, B-splines, and robust basis functions are 0.6686, 0.6708, 0.6662, and 0.6794, respectively (all within 2% of one another). This demonstrates that the significant improvement in mean and standard deviations of $e_{RMS}/y_{d,RMS}$ is achieved without significantly affecting nominal tracking accuracy of the FBF approach.

Since the uncertainty is concentrated around the resonance of the oscillator, the uncertainty will affect the tracking error only when the basis functions span the frequencies at or near the resonance. For DCT, BPF, and B-splines, as the number of basis functions increases, their bandwidth increases; for lower values of n, they span lower frequencies, and for higher values they span most of the frequency range. The DCT and BPF basis functions are

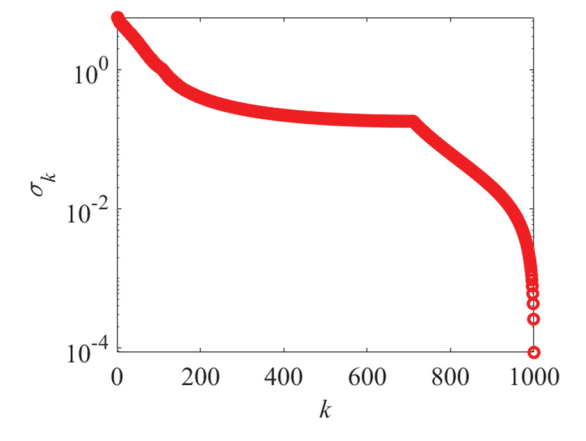


Fig. 6 Singular values of $-\Delta_{\text{nom},s}$

rudimentary basis functions in the frequency domain and time domain, respectively [10]. For lower values of n, the DCT basis functions only span the lower frequencies, whereas the BPF basis functions are pulses, which to some extent span higher frequencies. Hence, as seen in Fig. 5, the tracking accuracy of FBF for DCT is not affected by uncertainty for lower values of n, until the basis functions span the resonance frequencies. Once the bandwidth of DCT basis functions is greater than the resonance, the effect of uncertainty does not change much, and the standard deviation is mostly constant. Even for lower values of n, the pulsebased basis functions (BPF) span high frequencies to some extent and have nonzero standard deviation for lower values of n. As nincreases, the BPF basis functions have similar characteristics as DCT basis functions, beyond the resonance. In terms of frequency characteristics, B-splines lie between DCT and BPF. Hence, they start demonstrating nonzero standard deviation for values of ngreater than that demonstrated by BPF but for lower n than DCT basis functions. For lower values of n, the robust basis functions are designed to span the frequencies, which have minimal uncertainty, resulting in small deviation in the error, and as *n* increases, the effect of the uncertainty increases steadily, resulting in higher error (see Remark 8).

Figure 6 shows the singular values of $\bar{\Delta}_{nom,s}$ for the known uncertainty and nominal model. It is observed that the singular values are dispersed on either side of 1, and hence this case represents scenario (iii) in Remark 9. Using the singular values, the optimal value of *n* for the proposed robust optimal basis functions should be achieved at n = 891 (see Remark 9 for more details). The simulations (see Fig. 5) show that the minimum value of $mean(e_{RMS}/y_{d,RMS})$ for robust basis functions is achieved at n = 890. The values of mean($\mathbf{e}_{\text{RMS}}/\mathbf{y}_{d,\text{RMS}}$) for n = 890 and 891are 0.3935 and 0.394, respectively. This small difference in estimation of n could be attributed to the fact that the Frobenius norm metric only represents a trend and does not consider the effect of the desired trajectory. As compared to the other three basis functions, DCT, BPF, and B-splines, the robust basis functions achieve improvement in the minimum value of $mean(e_{RMS}/y_{d,RMS})$ by up to 1.8 times.

Figure 7 shows the normalized RMS control input $\mathbf{u}_{\text{RMS}}/\mathbf{y}_{d,\text{RMS}}$ for different types and number of basis functions (n=10–990). The maximum values of $\mathbf{u}_{\text{RMS}}/\mathbf{y}_{d,\text{RMS}}$, over n, for DCT, BPF, B-splines, and the robust basis functions are 1.1×10^3 , 1.21×10^1 , 7.64×10^9 , and 2.34×10^1 , respectively. The value of $\max(\mathbf{u}_{\text{RMS}}/\mathbf{y}_{d,\text{RMS}})$ is highest for B-splines, followed by DCT, robust, and BPF basis functions. The high values for B-splines and DCT can be attributed to the contribution of the very small singular value. The robust basis functions avoid the very small singular value due to the constraint formulation used for design of the basis functions

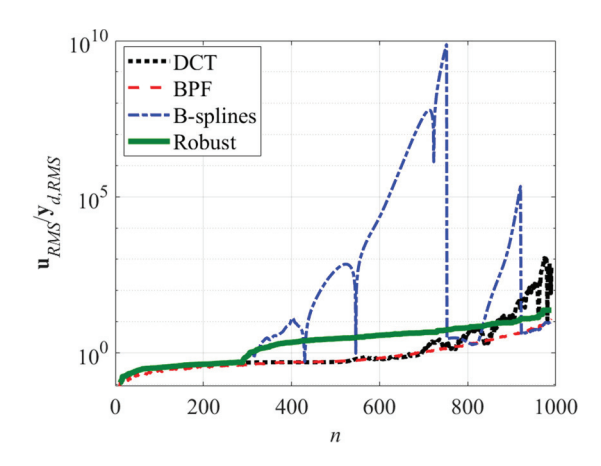


Fig. 7 Comparison of normalized RMS control effort for DCT, BPF, B-splines, and the robust basis functions, in the presence of uncertainty, for various values of number of basis functions, \boldsymbol{n}

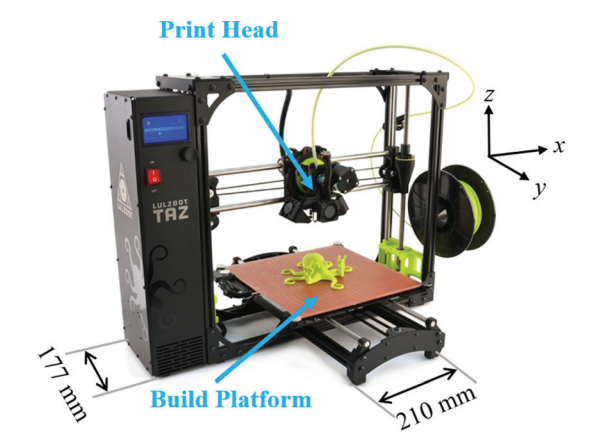


Fig. 8 Lulzbot Taz 6 desktop 3D printer

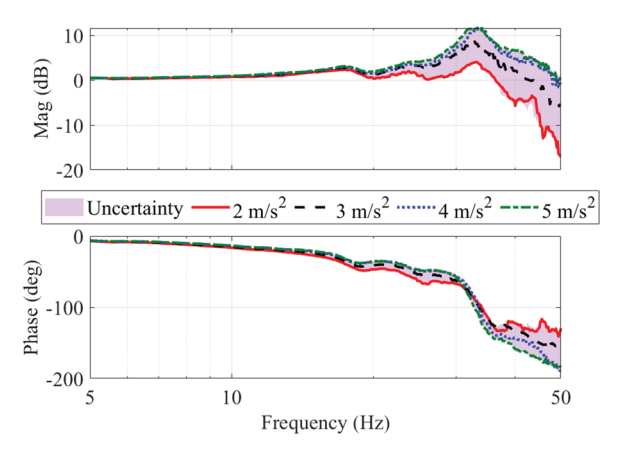


Fig. 9 Frequency response functions (FRFs) corresponding input acceleration levels $2\,\text{m/s}^2$, $3\,\text{m/s}^2$, $4\,\text{m/s}^2$, and $5\,\text{m/s}^2$, and uncertainty

(Proposition 3). The BPF basis functions result in the least control effort for the current example, but this cannot be guaranteed for all cases. Also, the maximum control effort required by BPF and robust basis functions is of the same order of magnitude. This demonstrates that the robust basis functions achieve large improvements in tracking accuracy without large increases in control effort, as compared to the popular basis functions in the literature.

4.2 Experiments. This section demonstrates the effectiveness of the robust basis functions as compared to B-splines using a Lulzbot Taz 6 desktop 3D printer (see Fig. 8). The FRFs of the 3D printer are obtained by applying swept sine acceleration signals (with amplitudes ranging from 2 m/s² to 5 m/s² in increments of $0.2 \,\mathrm{m/s^2}$) to the printer's stepper motors (each having $10 \,\mu\mathrm{m}$ stepping resolution) and measuring the relative acceleration of the build platform and print head using accelerometers (SparkFun ADXL335 triple-axis). Figure 9 shows the uncertainty and FRFs for 2 m/s², 3 m/s², 4 m/s², and 5 m/s². For robust FBF controller, the set $\{G_{ai}\}$ consists of the plant dynamics obtained from 16 FRFs (l = 16), corresponding to acceleration amplitudes 2–5 m/s² in increments of 0.2 m/s². For FRFs corresponding to 2 m/s² and 3 m/s², the corresponding LSRs do not have very small singular values (r=0), whereas, for FRFs corresponding to 4 m/s^2 and 5 m/s^2 , the LSRs have one very small singular value (r=1). The implication is that the set $\{G_{ai}\}$ contains minimum phase as well as NMP plants. The robust basis functions ($\lambda_i = 1/l$) are designed for nominal models based on FRFs corresponding to 2 m/s²,

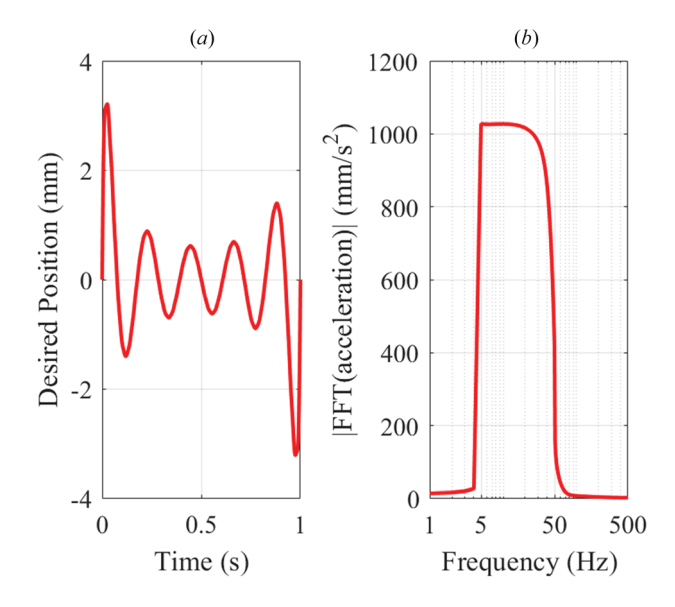


Fig. 10 (a) Desired position and (b) fast Fourier transform of its acceleration, to approximate operating condition corresponding to acceleration of 1 m/s²

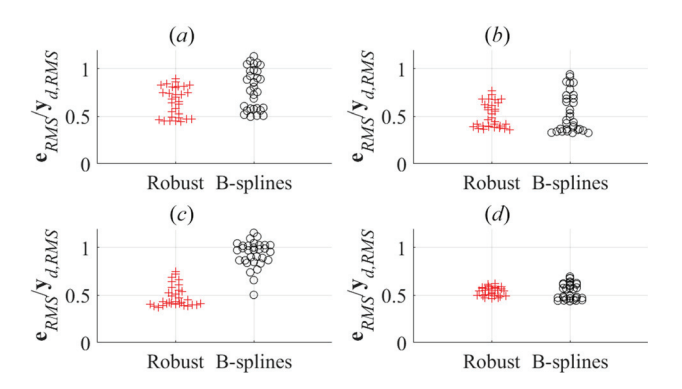


Fig. 11 Bee-swarm plots showing comparison of normalized RMS tracking error for robust basis functions and B-splines using four different nominal models: corresponding to (a) 2 m/s^2 FRF, (b) 3 m/s^2 FRF, (c) 4 m/s^2 FRF, and (d) 5 m/s^2 FRF (n = 100 and M = 1000)

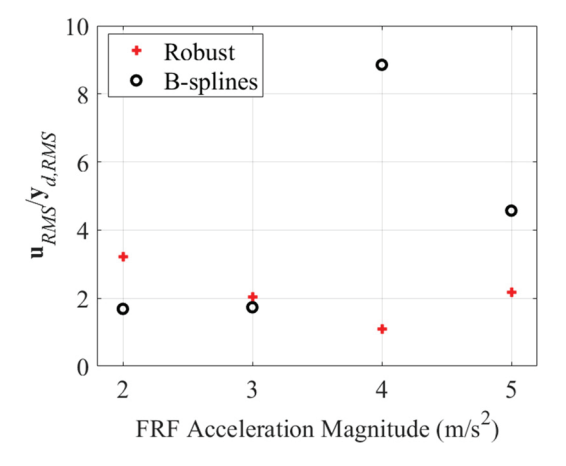


Fig. 12 Comparison of normalized RMS control input for robust basis functions and B-splines using four different nominal models: corresponding to $2\,\text{m/s}^2$ FRF, $3\,\text{m/s}^2$ FRF, $4\,\text{m/s}^2$ FRF, and $5\,\text{m/s}^2$ FRF (n=100 and M=1000)

 3 m/s^2 , 4 m/s^2 , and 5 m/s^2 . A signal with frequency content primarily distributed between 5 and 50 Hz is used as the desired trajectory (see Fig. 10). Such signals with high frequency content often occur when a 3D printer is rapidly tracing intricate contours with abrupt changes in direction [12,31]. The length of the signal is 1 s, resulting in 1001 discrete points (i.e., M = 1000) based on sampling time $T_s = 1 \text{ ms}$. The control inputs generated for various combinations of basis functions (n = 100) and nominal models are scaled and sent to the 3D printer to emulate 31 different uncertain plant dynamics. This essentially implies scaling the desired position to achieve operating conditions corresponding to accelerations of $2-5 \text{ m/s}^2$ in increments of 0.1 m/s^2 (resulting in 31 different uncertain dynamics). Figure 10 shows the desired position that approximates acceleration of 1 m/s^2 .

Figure 11 shows bee-swarm plots comparing the normalized RMS tracking error ($\mathbf{e}_{\text{RMS}}/\mathbf{y}_{d,\text{RMS}}$) for the proposed robust basis functions and B-splines using nominal models corresponding to FRFs of 2 m/s², 3 m/s², 4 m/s², and 5 m/s². It is observed that the robust basis functions perform better than B-splines in terms of mean as well as standard deviation. The robust basis functions improve the mean value of $\mathbf{e}_{\text{RMS}}/\mathbf{y}_{d,\text{RMS}}$ by 17%, 6%, 48%, and 1% for the FRFs corresponding to 2 m/s², 3 m/s², 4 m/s², and 5 m/s², respectively, as compared to B-splines, whereas the corresponding improvement in standard deviations is 27%, 38%, 20%, and 46%, respectively. Figure 12 shows the values of $\mathbf{u}_{\text{RMS}}/\mathbf{y}_{d,\text{RMS}}$ for B-splines and robust basis functions. The maximum value of $\mathbf{u}_{\text{RMS}}/\mathbf{y}_{d,\text{RMS}}$ for B-splines is 2.76 times the maximum value for the proposed basis functions which demonstrates that the robust basis functions are also preferable in terms of the control effort.

5 Conclusion and Future Work

The literature has shown that the FBF approach is an effective method for feedforward tracking control of linear (especially NMP) systems, assuming the plant model is known precisely. In reality, plant dynamics always has some uncertainty, and the tracking accuracy of feedforward methods such as FBF suffers in the presence of such uncertainty. However, unlike other methods in the literature, the FBF approach presents an additional tuning parameter, in the form of basis functions, which can be used to improve the tracking accuracy of the FBF approach in the presence of uncertainty.

Using a Frobenius norm metric, this paper studies the effect of known uncertainty and the choice of basis functions on the tracking accuracy of the FBF approach. The metric comprises of two components—nominal and uncertainty-related. The nominal component is independent of the plant dynamics and the type of basis functions. However, the uncertainty-related component depends on the known uncertainty, nominal model used for filtering the basis functions, and the type of basis functions. A robust set of basis functions that minimizes the effect of the uncertaintyrelated component, while maintaining the desired level of nominal component (nominal tracking accuracy) and bounds on control effort, is optimally selected. The robust basis functions ensure that the deviation in tracking error due to uncertainty from the nominal tracking accuracy is minimized for a large range of number of basis functions (Fig. 5). In many applications, this property could be useful in ensuring that the effective tracking property of the FBF approach is retained even in the presence of uncertainty.

In addition to basis functions and uncertainty, the tracking accuracy of the FBF approach also depends on the nominal model used for filtering the basis functions [31,38]; the nominal model also affects control effort. Future work will complement optimal selection of basis functions with optimal selection of nominal model to further enhance the tracking accuracy or reduce the control effort of the FBF approach in the presence of uncertainty. Future work will also focus on implementing the optimal basis functions and nominal model in a computational efficient manner,

e.g., using limited-preview optimization [12], to enable its use on lengthy trajectories used in 3D printing and other applications.

Funding Data

 National Science Foundation (CMMI 1825133: Boosting the Speed and Accuracy of Vibration-Prone Manufacturing Machines at Low Cost through Software; Funder ID: 10.13039/100000001).

Appendix A: Lifted System Representation

An LTI SISO causal plant G can be expressed as

$$G(q) = g_0 + g_1 q^{-1} + g_2 q^{-2} + \cdots$$
 (A1)

where the coefficients g_l are the Markov parameters of G. The sequence g_0, g_1, g_2, \ldots also represents the impulse response of G. Then

$$\begin{bmatrix}
y(0) \\
y(1) \\
\vdots \\
y(M)
\end{bmatrix} =
\begin{bmatrix}
g_0 & 0 & \dots & 0 \\
g_1 & g_0 & \dots & 0 \\
\vdots & \vdots & \ddots & \vdots \\
g_M & g_{M-1} & \dots & g_0
\end{bmatrix}
\begin{bmatrix}
u(0) \\
u(1) \\
\vdots \\
u(M)
\end{bmatrix}$$
(A2)

For an LTI noncausal controller C

$$C(q) = \dots + c_{-2}q^2 + c_{-1}q^1 + c_0 + c_1q^{-1} + c_2q^{-2} + \dots$$
 (A3)

the LSR of C can be expressed as

$$\underbrace{\begin{bmatrix} u(0) \\ u(1) \\ \vdots \\ u(M) \end{bmatrix}}_{\mathbf{u}} = \underbrace{\begin{bmatrix} c_0 & c_{-1} & \dots & c_{-M} \\ c_1 & c_0 & \dots & c_{-M+1} \\ \vdots & \vdots & \ddots & \vdots \\ c_M & c_{M-1} & \dots & c_0 \end{bmatrix}}_{\mathbf{y}_d} \underbrace{\begin{bmatrix} y_d(0) \\ y_d(1) \\ \vdots \\ y_d(M) \end{bmatrix}}_{\mathbf{y}_d}$$
(A4)

Similarly, overall dynamics L and error dynamics $E_{\rm ff}$ can be expressed in LSR as L and $E_{\rm ff}$. For LTI systems, the LSR is Toeplitz. For LTV systems or controllers, the construction of the LSR for L and $E_{\rm ff}$ follows a similar process but the resulting matrices are not Toeplitz [39].

Appendix B: Basis Functions

The DCT is a frequency-based transform that is widely used in signal processing; its basis functions are real-valued cosines defined as [28]

$$\varphi_{i}(k) = \beta_{i} \cos\left(\frac{\pi(2k+1)i}{2(M+1)}\right); \ \beta_{i} = \begin{cases} \frac{1}{\sqrt{M+1}} & i = 0\\ \sqrt{\frac{2}{M+1}} & i > 0 \end{cases}$$
(B1)

The BPF basis functions are given by

$$\varphi_{i}(k) = \begin{cases} & k \in \left[i\frac{M}{n+1}, (i+1)\frac{M}{n+1}\right), 0 \le i < n \\ & \text{and } k \in \left[i\frac{M}{n+1}, (i+1)\frac{M}{n+1}\right], i = n \\ & \text{otherwise} \end{cases}$$
(B2)

The BPF expressed in Eq. (B2) seeks to divide the time interval from 0 to M among n+1 basis functions in a quasi-uniform manner

For a B-spline of degree m, having $n+1 \le M+1$ control points (same as coefficients of basis functions), $\gamma_0, \gamma_1, ..., \gamma_n$, and knot vector $[\eta_0, \eta_1, ..., \eta_{m+n+1}]^T$, its real-valued basis functions, $\varphi_{i,m}$, are given by [36]

e given by [36]
$$\varphi_i(k) := \varphi_{i,m}(\xi_k) = \frac{\xi_k - \eta_i}{\eta_{i+m} - \eta_i} \varphi_{i,m-1}(\xi) + \frac{\eta_{i+m+1} - \xi_k}{\eta_{i+m+1} - \eta_{i+1}}$$

$$\varphi_{i+1,m-1}(\xi)$$

$$\varphi_{i,0}(\xi_k) = \begin{cases} 1 & \eta_i \le \xi_k \le \eta_{i+1} \\ 0 & \text{otherwise} \end{cases}$$

where i = 0, 1, ..., n with $\xi_k \in [0,1]$, representing normalized time, discretized into M+1 points, $\xi_0, \xi_1, ..., \xi_M$, and η_i is a uniform knot vector, selected such that

$$\eta_{j} = \begin{cases}
0 & 0 \le j \le m \\
\frac{j-m}{n-m+1} & m+1 \le j \le n \\
1 & n+1 \le j \le m+n+1
\end{cases}$$
(B4)

(B3)

References

- [1] Bruijnen, D., and van Dijk, N., 2012, "Combined Input Shaping and Feedforward Control for Flexible Motion Systems," Proceedings of the 2012 American Control Conference, Montreal, QC, Canada, June 27–29, pp. 2473–2478.
- [2] Tomizuka, M., 1987, "Zero Phase Error Tracking Algorithm for Digital Control," ASME J. Dyn. Syst., Meas., Control, **109**(1), pp. 65–68.
 [3] Faanes, A., and Skogestad, S., 2004, "Feedforward Control Under the Presence
- of Uncertainty," Eur. J. Control, 10(1), pp. 30-46.
- [4] Astrom, K., and Wittenmark, B., 1984, Computer Controlled Systems: Theory and Design, Prentice Hall, Upper Saddle River, NJ.
- [5] Miu, D. K., 2012, Mechatronics: Electromechanics and Contromechanics, Springer Science & Business Media, New York.
- [6] Clayton, G. M., Tien, S., Leang, K. K., Zou, Q., and Devasia, S., 2009, "A Review of Feedforward Control Approaches in Nanopositioning for High-
- Speed SPM," ASME J. Dyn. Syst., Meas., Control, **131**(6), p. 061101.
 [7] Rigney, B. P., Pao, L. Y., and Lawrence, D. A., 2009, "Nonminimum Phase Dynamic Inversion for Settle Time Applications," IEEE Trans. Control Syst. Technol., 17(5), pp. 989-1005.
- [8] van Zundert, J., and Oomen, T., 2018, "On Inversion-Based Approaches for Feedforward and ILC," Mechatronics, 50, pp. 282-291.
- [9] Duan, M., Ramani, K. S., and Okwudire, C. E., 2015, "Tracking Control of Non-Minimum Phase Systems Using Filtered Basis Functions: A NURBS-Based Approach," ASME Paper No. DSCC2015-9859.
- [10] Ramani, K. S., Duan, M., Okwudire, C. E., and Ulsoy, A. G., 2017, "Tracking Control of Linear Time-Invariant Nonminimum Phase Systems Using Filtered Basis Functions," ASME J. Dyn. Syst., Meas., Control, 139(1), p. 011001.
- [11] Kasemsinsup, Y., Romagnoli, R., Heertjes, M., Weiland, S., and Butler, H., 2017, "Reference-Tracking Feedforward Control Design for Linear Dynamical Systems Through Signal Decomposition," American Control Conference (ACC), Seattle, WA, May 24-26, pp. 2387-2392.
- [12] Duan, M., Yoon, D., and Okwudire, C. E., 2018, "A Limited-Preview Filtered B-Spline Approach to Tracking Control-With Application to Vibration-Induced Error Compensation of a Commercial 3D Printer," Mechatronics, 56, pp. 287-296.
- [13] Romagnoli, R., and Garone, E., 2019, "A General Framework for Approxi-
- mated Model Stable Inversion," Automatica, 101, pp. 182–189.
 [14] Frueh, J. A., and Phan, M. Q., 2000, "Linear Quadratic Optimal Learning Control (LQL)," Int. J. Control, 73(10), pp. 832-839.
- [15] Ramani, K. S., Duan, M., Okwudire, C. E., and Ulsoy, A. G., 2018, "A Lifted Domain-Based Metric for Performance Evaluation of LTI and LTV Discrete-

- Time Tracking Controllers," 2018 International Symposium on Flexible Automation, Kanazawa, Japan, pp. 248-255.
- [16] Zhao, Y., and Jayasuriya, S., 1995, "Feedforward Controllers and Tracking Accuracy in the Presence of Plant Uncertainties," ASME J. Dyn. Syst., Meas Control, 117(4), pp. 490-495.
- [17] Tsao, T.-C., and Tomizuka, M., 1987, "Adaptive Zero Phase Error Tracking Algorithm for Digital Control," ASME J. Dyn. Syst., Meas., Control, 109(4), pp. 349-354.
- [18] Adam, E. J., and Marchetti, J. L., 2004, "Designing and Tuning Robust Feedforward Controllers," Comput. Chem. Eng., 28(9), pp. 1899–1911
- [19] Devasia, S., 2002, "Should Model-Based Inverse Inputs Be Used as Feedforward Under Plant Uncertainty?," IEEE Trans. Autom. Control, 47(11), pp. 1865–1871.
- [20] Wu, Y., and Zou, Q., 2009, "Robust Inversion-Based 2-DOF Control Design for Output Tracking: Piezoelectric-Actuator Example," IEEE Trans. Control Syst. Technol., 17(5), pp. 1069–1082.
- [21] Lunenburg, J. J. M., 2010, "Inversion-Based MIMO Feedforward Design Beyond Rigid Body Systems," Eindhoven University of Technology, Eindhoven, The Netherlands, Technical Report No. 2010.061.
- [22] Pao, L. Y., Butterworth, J. A., and Abramovitch, D. Y., 2007, "Combined Feedforward/Feedback Control of Atomic Force Microscopes," 2007 American Control Conference, New York, July 11-13, pp. 3509-3515.
- [23] Aphale, S. S., Devasia, S., and Moheimani, S. R., 2008, "High-Bandwidth Control of a Piezoelectric Nanopositioning Stage in the Presence of Plant Uncertainties," Nanotechnology, 19(12), p. 125503.
- Wu, Y., and Zou, Q., 2009, "An Iterative-Based Feedforward-Feedback Control Approach to High-Speed Atomic Force Microscope Imaging," ASME J. Dyn. Syst., Meas., Control, 131(6), p. 061105.
- [25] Wang, H., Kim, K., and Zou, Q., 2013, "B-Spline-Decomposition-Based Output Tracking With Preview for Nonminimum-Phase Linear Systems," Automatica, **49**(5), pp. 1295–1303.
- [26] de Rozario, R., Fleming, A. J., and Oomen, T., 2016, "Iterative Control for Periodic Tasks With Robustness Considerations, Applied to a Nanopositioning Stage," IFAC-PapersOnLine, 49(21), pp. 623-628.
- [27] Tayebi, A., Abdul, S., Zaremba, M., and Ye, Y., 2008, "Robust Iterative Learning Control Design: Application to a Robot Manipulator," IEEE/ASME Trans. Mechatronics, 13(5), pp. 608-613.
- Ye, Y., and Wang, D., 2005, "DCT Basis Function Learning Control," IEEE/ ASME Trans. Mechatronics, 10(4), pp. 449–454.
- [29] Ramani, K. S., and Okwudire, C. E., 2016, "Regularized Filtered Basis Functions Approach for Accurate Tracking of Discrete-Time Linear Time Invariant Systems With Bounded Random Uncertainties," ASME Paper No. DSCC2016-
- [30] Ramani, K. S., and Okwudire, C. E., 2018, "Robust Filtered Basis Functions Approach for Feedforward Tracking Control," ASME Paper No. DSCC2018-
- [31] Ramani, K. S., Edoimioya, N., and Okwudire, C. E., 2020, "A Robust Filtered Basis Functions Approach for Feedforward Tracking Control-With Application to a Vibration-Prone 3D Printer," IEEE/ASME Trans. Mechatronics, 25(5), pp. 2556-2564.
- [32] Ramani, K. S., Duan, M., Okwudire, C. E., and Ulsoy, A. G., 2019, "Optimal Selection of Basis Functions for Minimum-Effort Tracking Control of Nonminimum Phase Systems Using Filtered Basis Functions," ASME J. Dyn. Syst., Meas., Control, 141(11), p. 111009.
- [33] Ramani, K. S., and Okwudire, C. E., 2020, "Optimal Selection of Basis Functions for Robust Tracking Control of Linear Systems Using Filtered Basis Functions," American Control Conference (ACC), Denver, CO, pp. 1539-1544.
- [34] Gross, E., Tomizuka, M., and Messner, W., 1994, "Cancellation of Discrete Time Unstable Zeros by Feedforward Control," ASME J. Dyn. Syst., Meas., Control, 116(1), pp. 33-38.
- [35] Deb, A., Sarkar, G., and Sen, S. K., 1994, "Block Pulse Functions, the Most Fundamental of All Piecewise Constant Basis Functions," Int. J. Syst. Sci., 25(2), pp. 351-363.
- [36] Piegl, L., and Tiller, W., 1997, The NURBS Book, Springer, New York.
- [37] Yoon, D., Ge, X., and Okwudire, C. E., 2019, "Optimal Inversion-Based Iterative Learning Control for Overactuated Systems," IEEE Trans. Control Syst. Technol., 28(5), pp. 1948–1955.
- [38] Ramani, K. S., and Okwudire, C. E., 2020, "Two-Stage Robust Tracking Controller for Linear Systems With Known Uncertainty Using Filtered Basis Functions," ASME Paper No. DSCC2020-3207.
- Bristow, D. A., Tharayil, M., and Alleyne, A. G., 2006, "A Survey of Iterative Learning Control," IEEE Control Syst. Mag., 26(3), pp. 96-114.